Sequential *in situ* STM imaging of electrodissolving copper single-crystal domains in aqueous perchloric acid: Kinetics and mechanism of the interface evolution

S. G. Aziz,* M. E. Vela, G. Andreasen, R. C. Salvarezza, A. Hernández-Creus,† and A. J. Arvia
Instituto de Investigaciones Fisicoquímicas Teóricas y Aplicadas (INIFTA), Sucursal 4, Casilla de Correo 16, 1900 La Plata, Argentina

(Received 5 August 1996; revised manuscript received 10 January 1997)

The evolution of Cu crystal surfaces in an aqueous perchloric acid solution at both null ($j=0$) and constant anodic apparent current density ($j=6\ \mu\mathrm{A\ cm^{-2}}$) at room temperature was followed by *in situ* scanning tunneling microscopy sequential imaging. For $j=0$, the Cu surface turns out to be highly dynamic as terrace growth, step displacement, and smoothening of small pits can be observed. These processes lead to a small decrease in the value of the root-mean-square roughness (ξ). On the other hand, for $j=6\ \mu\mathrm{A\ cm^{-2}}$, an inhomogeneous attack proceeds with a marked increase in ξ. In this case, while some surface domains become progressively rough others develop nm-sized etched pits that turn the interface unstable. The evolution of the Cu topography under the experimental conditions of this work was simulated using a Monte Carlo algorithm based on a dissolution model in which surface processes are influenced by inhomogeneity stabilizing cavities. [S0163-1829(97)07831-4]

I. INTRODUCTION

The morphological aspects of processes involving the removal of material from surfaces that are important in a wide range of applications have received considerably little attention as compared to surface morphology in deposition and growth processes, except in very recent papers dealing with either theoretical models or experimental data related to a few systems.[1,2]

Solid attack in aggressive environments involves a number of processes generally leading to the loss of material and appearance of an irregular surface topography. In such a case, the development of a particular topography results from a competition among different physical processes associated with the displacement of the interface. Considering a relatively simple framework, a self-affine fractal surface is expected when solid dissolution or growth is dominated by surface processes, whereas an unstable interface is produced when surface processes are coupled with either electrical or concentration fields operating in the environment around the interface.[3]

On the other hand, the kinetics and mechanism of metal dissolution, particularly oriented towards corrosion processes in aqueous solutions, have been extensively considered for a long time.[4] Commonly, at low dissolution rates, the kinetics of these reactions is dominated by surface processes involving interfacial charge transfer that occur mainly at surface sites where atoms in the lattice are more weakly bound. The number of such active sites depends on the structure and morphology of the corroding surface, and vice versa, the morphology of the corroding surface reflects in some way the kinetics and mechanism of the overall process.

In contrast to surface crystallography, surface morphology has not been specifically considered in most theories of metal dissolution and electrodissolution in aggressive media,[4,5] as kinetic descriptions usually include average kinetic parameters in the relationships between the reaction rate and the activation energy. In fact, due to the stochastic nature of the dynamics of metal dissolution, surface morphology is expected to change with time, in many cases evolving into rough structures which have a considerable influence on the overall reaction.[6]

For a solid-phase growth far from equilibrium, the kinetics of the interface roughening is enhanced, and in these cases, even the possibility of a transition in the kinetics of roughening has been investigated.[6–9] This transition is the nonequilibrium analog of the equilibrium roughness transition which is known to occur for phase growth on low-index metal surfaces. While growth on flat surfaces is only possible via nucleation processes, rough surfaces feature a continuous regime leading to irregular topographies with fractal surface characteristics.[10] The same situations should be expected for a solid-phase disruption.

Computer models of chemical dissolution including the influence of the applied potential[6] have been advanced by a number of authors.[11–13] In these cases, roughness may induce a change in the dissolution mechanism from one at low overvoltages characterized by kink propagation at steps to one at large overvoltages where low coordination sites actively participate in the processes.

Surface roughness of corroding metal surfaces initiated on a flat substrate has been shown to exhibit a scaling behavior over a wide variation in length scales, a fact which has aroused considerable interest in the physics of dynamic scaling.[14–16]

The dynamic scaling theory predicts that the interface width, i.e., the mean surface height fluctuation $\xi(L,t)$, for length scale L and growth time t, scales as[16,17]

$$\xi(L,t)\propto t^{\beta} f(t/L^{\alpha/\beta}). \tag{1}$$

Equation (1) for $t\gg L^{\alpha/\beta}$ becomes

$$\xi(L,t)\propto L^{\alpha}, \tag{2}$$

while for $t\ll L^{\alpha/\beta}$

$$\xi(L,t) \propto t^{\beta}. \tag{3}$$

In Eqs. (1)–(3) β and α are called the growth and roughness exponents, respectively. The value of α is related to the surface texture, and hence to D, the fractal surface dimension of the self-affine surface, by $D=3-\alpha$. Thus, for $\alpha \Rightarrow 1$ ($D \Rightarrow 2$), the surface tends to be Euclidean (ordered), whereas, when $\alpha \Rightarrow 0$ ($D \Rightarrow 3$), the surface exhibits an increasing degree of disorder. It should be noted that the exponents α and β are not independent and there is a simple way to ''collapse'' the temporal and spatial ξ data onto a single curve by plotting ξ/L^{α} versus $t/L^{\alpha/\beta}$.[3]

In many cases, key parameters α and β can be derived from the analysis of surface profiles resulting from adequate imaging procedures, such as those profiles derived from scanning tunneling microscopy (STM) images which provide high lateral resolution three-dimensional (3D) images in real space. Equations (1)–(3) can be extended to data on STM images by replacing ξ by ξ_{STM}, the root-mean-square roughness resulting from STM profiles, and L by L_s, a segment of the STM scan.[17,18] The values of α and β can be compared to those derived from atomistic and continuum models for interface evolution.[2] However, the interface evolution becomes unstable when its motion is influenced by a Laplacian field built around the moving interface. In this case, the topography of the interface is no longer a self-affine fractal, and then the dynamic scaling theory is no longer applicable.

Roughness evolution during the electrodissolution of Ag single-crystal surfaces in contact with aqueous $1M$ $HClO_4$ under surface reaction control has been recently reported based on *in situ* sequential STM imaging.[2] It has been shown that for low current densities ($j<15\ \mu\mathrm{A\ cm^{-2}}$), Ag electrodissolution proceeds without significant surface roughening, whereas for higher electrodissolution rates ($j>15\ \mu\mathrm{A\ cm^{-2}}$) both void formation and smoothening can be observed. The dynamic scaling analysis of STM images[18] resulting from $j>15\ \mu\mathrm{A\ cm^{-2}}$ leads to $\beta=0.36$, and $\alpha=0.9$. This value of α indicates that the Ag topography results from an electrochemical surface reaction in which Ag surface-atom diffusion plays a key role, whereas the value $\beta \cong 0.36$ would reflect the influence of energy barriers at step edges which hinder interlayer mass transport.[19] On the other hand, for $j<15\ \mu\mathrm{A\ cm^{-2}}$, Ag electrodissolution proceeds from step edges leading to layer-by-layer dissolution ($\beta \cong 0$).

Data from investigations on Cu electrodes, particularly on the nucleation and growth of Cu deposits, which have been carried out in the Cu/Cu,[20] Cu/Au,[21,22] and Cu/Pt (Ref. 23) systems, compare well with the $3d$ nucleation theory at large cathodic overvoltages. However, *in situ* atomic force microscopy (AFM) results have shown that a more detailed theory is required, particularly at low cathodic overvoltages in which the contribution of surface imperfections, such as steps and kinks, plays a crucial role in the process.[21,23–25] The dynamic scaling behavior of Cu, growth in a stirred aqueous $CuSO_4$ solution at low growth rates has also been investigated.[26]

On the other hand, the anodic dissolution of Cu in aqueous $0.01M$ $CuSO_4+0.01\ M$ H_2SO_4 has been studied by *in situ* STM from a deposit of μm-sized bulk crystals produced on a Au substrate.[22] The dissolution of Cu is characterized by an initial rapid change in Cu morphology from μm-sized crystals to faceted structures, as found for Cu anodized in aqueous H_2SO_4 (Ref. 27) and aqueous $HClO_4$ solution.[20] It has been concluded that, in these cases, the average anodic current peak usually found for Cu electrodissolution does not reflect a simple process of Cu oxidation. This aspect of the problem is explored in this work, which describes the evolution of the topography of Cu(111) domains in contact with an aqueous perchloric acid under a constant anodic apparent current density (j) resulting from *in situ* STM sequential imaging, considering the potential range where the electrochemical reaction is under a surface reaction kinetic control.

For $j=0$, the Cu surface becomes highly dynamic, as can be seen by terrace growth, step displacement, and pit smoothening, whereas for $j=6\ \mu\mathrm{A\ cm^{-2}}$ Cu electrodissolution proceeds inhomogeneously yielding an irregular topography. In this case, surface roughening is accompanied by the development of etched pits which drive the surface evolution to an unstable roughness regime with $\beta > \frac{1}{2}$. The evolution of the topography of the electrodissolving Cu surface in an aqueous $HClO_4$ solution can account for a dissolution model involving surface processes influenced by inhomogeneity stabilizing cavities.

II. EXPERIMENT

Cu electrodissolution was performed in the electrochemical setup provided with the Nanoscope III STM (Digital Instruments, Santa Barbara, CA) equipment, which consisted of a small Kel-F cell ($1.1\times 2.0\ \mathrm{cm^2}$ in size) provided with a polycrystalline Cu plate (99.99% purity) working electrode (exposed area $0.5\ \mathrm{cm^2}$), a large Pt counter electrode, and a $Pd/H_2/H^+$ reference electrode. The working electrode was first mechanically polished, and then annealed at 400 °C under a H_2 atmosphere to obtain Cu surfaces formed by smooth terraces and steps only a few atoms in height. The STM images of these electrodes showed μm-sized ordered terrace domains with well-defined steps intersecting at angles close to 60°, as expected from a Cu(111) surface. These topographic features made it possible to select smooth single-crystal domains $2000\times 2000\ \mathrm{nm^2}$ in size whose topographic changes could be followed by sequential *in situ* STM imaging.

Runs were made at $T=298\ \mathrm{K}$ in aqueous $1M$ $HClO_4$. This solution was prepared from 70% ar-quality $HClO_4$ and Milli-Q* water and deaerated with purified N_2. To avoid air incorporation into the solution, both the electrochemical cell and the STM head were placed in a glass chamber under a continuous flow of purified N_2.

The conventional voltammetric response of the nonequilibrium Cu/aqueous $1M$ $HClO_4$ system was obtained at the potential sweep rates $v=10^{-3}$ and $2\times 10^{-2}\ \mathrm{V\ s^{-1}}$, covering the potential range -0.15 to 0.4 V. The convenient potential window for *in situ* STM imaging was selected in this way. All potentials in the text are referred to the standard hydrogen electrode (SHE) scale.

Cu electrodissolution runs for sequential *in situ* STM imaging were performed in the following way. First, the working electrode was polarized at $E=-0.05$ V, i.e., a potential at which no Cu electrodissolution takes place ($j=0$). Afterwards, a smooth surface domain, typically $2000\times 2000\ \mathrm{nm^2}$

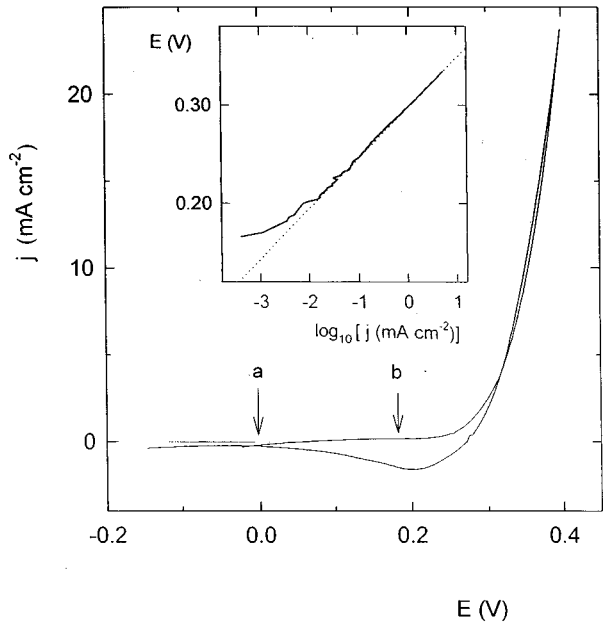

FIG. 1. (a) A voltammogram of a Cu electrode in $1M$ $HClO_4$ recorded at 0.02 V s^{-1} between -0.15 and 0.4 V $T=298$ K. A typical E vs $\log_{10} j$ curve obtained at 0.001 V/s with a Cu electrode in $1M$ $HClO_4$ at $T=298$ K is shown as an inset.

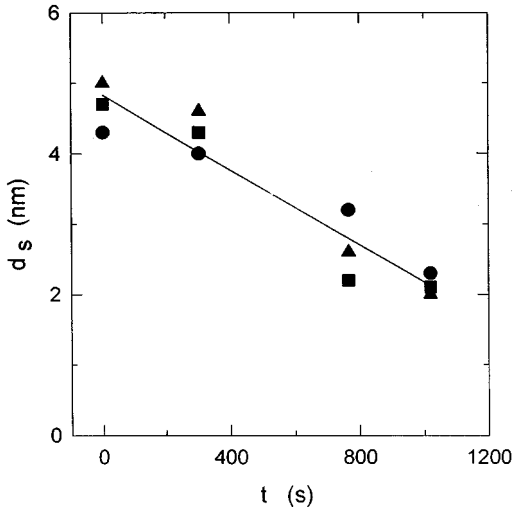

FIG. 2. A d_s vs t plot for different small rounded pits.

in size, was chosen, and after drift attenuation, a series of STM images of this domain were taken for 20 min at null net current to check, under this condition, the root-mean-square roughness, which was typically 1 nm. Later, Cu electrodissolution at $j=6$ μA cm^{-2} proceeded simultaneously with the sequential *in situ* STM imaging from $t=0$, i.e., when the electrodissolution current was switched on, up to $t=1600$ s.

STM imaging was made using Pt-Ir nanotips covered by Apiezon wax to minimize the possible interference of faradaic currents. The following conditions for *in situ* STM imaging were used. The tip potential covered the range $0.10 \leqslant E_t \leqslant 0.35$ V; the tunneling current was $I_t=2$ nA, the bias voltage was $E_b=0.1$ V, and the scanning rate was 5 Hz. The value of E_t was always in the double-layer potential range of the tip material in the solution. It was chosen sufficiently positive to avoid electrodeposition of dissolving Cu from the substrate on the tip.

STM data were analyzed after instrument plane removal, as described elsewhere.[18,28]

Occasionally *ex situ* AFM imaging of the Cu surface was also made to disregard the presence of tip-induced artifacts during the *in situ* STM imaging. These runs were made using a Nanoscope III AFM equipment (Digital Instruments, Santa Barbara, CA) operating in the contact mode. Au cantilevers with integral Si_3N_4 tips were used. Typical forces used in these measurements were 10 nN.

III. RESULTS AND INTERPRETATION

A. Electrochemical data

The voltammogram of polycrystalline Cu in aqueous $1M$ $HClO_4$ run at $v=0.02$ V s^{-1} from -0.15 to 0.40 V (Fig. 1) shows a null current from -0.15 to 0.15 V followed by a fast anodic current increase with E that corresponds to Cu electrodissolution. Subsequently, the reverse potential scan exhibits a broad cathodic current peak at $E=0.20$ V, which is related to the electroreduction of soluble Cu species previously formed. The $\ln j_{10}$ versus E plot resulting from anodic polarization at $v=10^{-3}$ V s^{-1} yields a straight line with a slope $b_a \cong 0.040$ V $decade^{-1}$ (Fig. 1, inset), in agreement with data already reported in the literature.[29] The arrows denoted by a and b in Fig. 1 indicate the values of j chosen for the *in situ* STM imaging.

B. STM imaging at a null faradaic current

The *in situ* STM image (topographic mode) 1700×1700 nm^2 in size of a Cu single-crystal domain immersed in the working solution, taken a null current (arrow a in Fig. 1), shows terraces with steps intersecting at 60° angles. A large number of homogeneously distributed bumps and occasionally a few rounded pits 70–100 nm in size and 2–5 nm in depth can be seen on terraces. The *in situ* STM sequential images and their corresponding cross sections reveal a progressive growth of small facets at the expense of bumps and a decrease in the depth (d_s) and pit radius (r) of small rounded pits. As already reported for Au electrodes in acid solutions, the value of d_s measured from the STM cross sections decreases almost linearly with the immersion time (Fig. 2) leading to a filling rate close to 0.003 nm/s.

Let us assume that the pit filling rate is under a surface diffusion-controlled process, then the following relationship holds:[30]

$$\Delta r^2 = 2Dt_f, \tag{4}$$

where t_f is the time required for filling a substrate monolayer taken from the slope of the linear d_s versus t plot (Fig. 2), Δr is the decrease in pit radius defined as $r(t_f=0)$ and $r(t_f)$, and D is the surface diffusion coefficient of Cu atoms. From Eq. (4) $D \cong 10^{-15}$ cm^2 s^{-1} for Cu in the acid electrolyte at $E \cong -0.05$ V.

The surface mobility of Cu atoms that is reflected in facet growth, step displacement, and pit filling leads to a slight

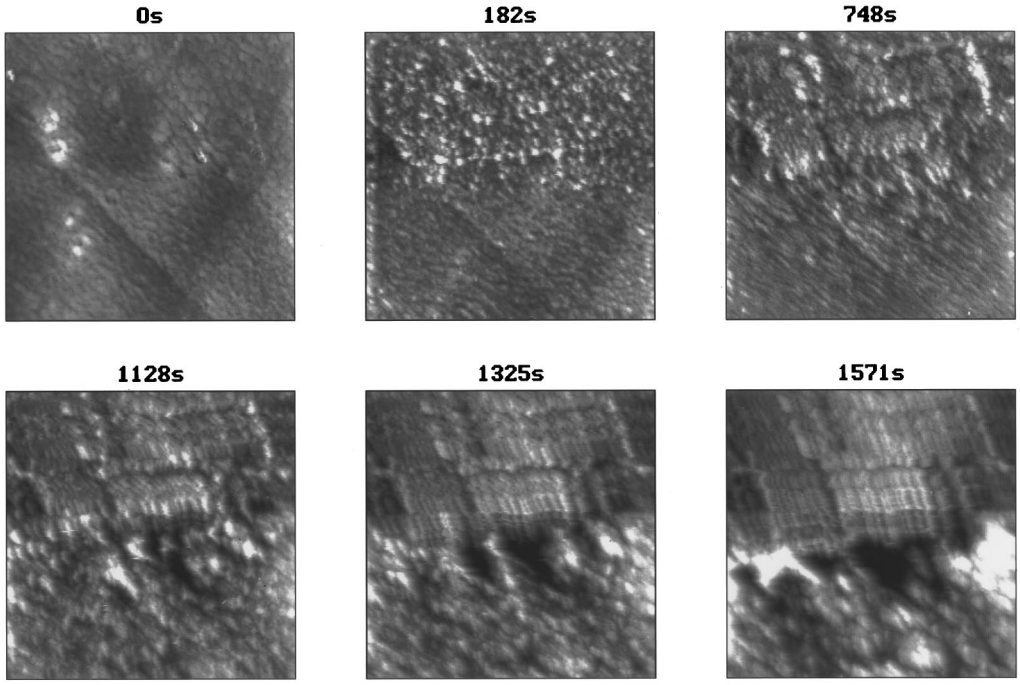

FIG. 3. Sequential STM images (top view) ($1700 \times 1700\ \mathrm{nm}^2$) obtained during the electrodissolution of Cu in $1M$ $HClO_4$ at $j = 6\ \mu\mathrm{A\ cm}^{-2}$. The electrodissolution time is indicated in the upper part of each picture. The image shown in (a) was taken immediately after E was changed from $E = -0.05$ V to $E = 0.2$ V ($t = 0$). $T = 298$ K.

decrease in the ξ_{STM} value from $\xi_{\mathrm{STM}} = 1$ nm ($t = 0$) to $\xi_{\mathrm{STM}} = 0.6$ ($t = 20$ min) for the Cu electrode immersed in the acid solution at null current.

C. STM imaging at a constant electrodissolution current

A similar set of STM images [Figs. 3(a)–3(f)] made under $j = 6\ \mu\mathrm{A\ cm}^{-2}$ (arrow *b* in Fig. 1) shows the rapid disappearance of steps and the progressive development of an irregular topography which results in different surface domains. Thus, the upper part of STM images exhibits a gradual development of a facetted structure (domain I), whereas their lower part shows the development of a bump structure (domain II), and their central part reveals the formation of deep etched pits (domain III), which are located in between domains I and II. As seen in Figs. 3(a)–3(f), etched pit formation involves an induction time (t_i) of at least 700 s. The topographic characteristics in the z direction of these domains can be clearly distinguished from the cross sections of STM images at advanced dissolution times [Figs. 4(a)–4(c)]. It is evident that domains I and II involve the development of irregularities that grow more slowly than the deep etched pits shown in domain III. The growth of etched pits can be followed by analyzing the time dependence of STM image cross sections of the corroding Cu surface both on the x-z and y-z plane [Fig. 4(c)]. Thus, the value of d, the etched pit depth, after t_i, increases almost linearly with t. The average etched pit penetration rate in terms of the number of dissolved Cu atoms per second, derived from the slope of the linear portion of the d versus t plot, can be estimated as 0.2 atom s^{-1}.

Domains I and II, where etched pits are absent, become rougher as the electrodissolution process proceeds, as can be concluded from the evolution of the surface profile [Fig. 5(a)]. For these domains no reliable value of β from the $\log_{10} \xi_{\mathrm{STM}}$ versus $\log_{10} t$ plot [Fig. 5(b)] could be obtained because of data scattering. The only conclusion derived from this plot is that the value of β is very likely comprised in the range $\frac{1}{4} \leqslant \beta \leqslant \frac{1}{2}$ [Fig. 5(b)].

On the other hand, the overall interface evolution (domains I, II, and III) resulting from Cu immersed in the acid solution under $j = 6\ \mu\mathrm{A\ cm}^{-2}$ can be conveniently expressed by the change in ξ_{STM} resulting from STM images. For the images shown in Figs. 3(a)–3(f), the ξ_{STM} versus t plot [Fig. 5(c)] exhibits an initial slight increase but for $t > t_i$ the value of ξ_{STM} increases markedly without reaching a limiting value, as should be expected for a stable roughness regime. In this case, for the unstable interface the proportionality $\xi_{\mathrm{STM}} \propto t^{\beta}$ with $\beta > \frac{1}{2}$ is approached. Therefore, as there is a clear correlation between the evolution of d and the final evolution of ξ_{STM} [Fig. 5(c)], it is reasonable to conclude that for the overall interface evolution ξ_{STM} is dominated by etched pits (singularities). It is worth noting that for unstable surfaces the value of α is undeterminable and the dynamic scaling approach breaks down.

To discard the possibility that the development of etched pits under *in situ* STM imaging could be assigned to a tip-induced artifact, Cu electrodes were anodized for 30 min at $j = 6\ \mu\mathrm{A\ cm}^{-2}$ in a conventional electrochemical cell, and subsequently, the topography of the electrode was imaged *ex situ* by AFM (Fig. 6). These images show the same type of etched pits already described from *in situ* STM images. Consequently, a tip-induced artifact must be discarded as the origin of etched pit formation on Cu in the acid solution.

Furthermore, to discard also the possibility that pit formation could be caused by traces of Cl^- anions usually present in aqueous $HClO_4$ solutions, similar experiments were made by anodizing Cu in aqueous $0.5M$ H_2SO_4. In this case, the formation of etched pits similar to those described for aqueous $1M$ $HClO_4$ could be observed.

IV. DISCUSSION

A. Surface diffusion and roughening

The preceding analysis of experimental results emphasized two relevant features related to the Cu/aqueous solution interface, namely, the relatively high mobility of Cu

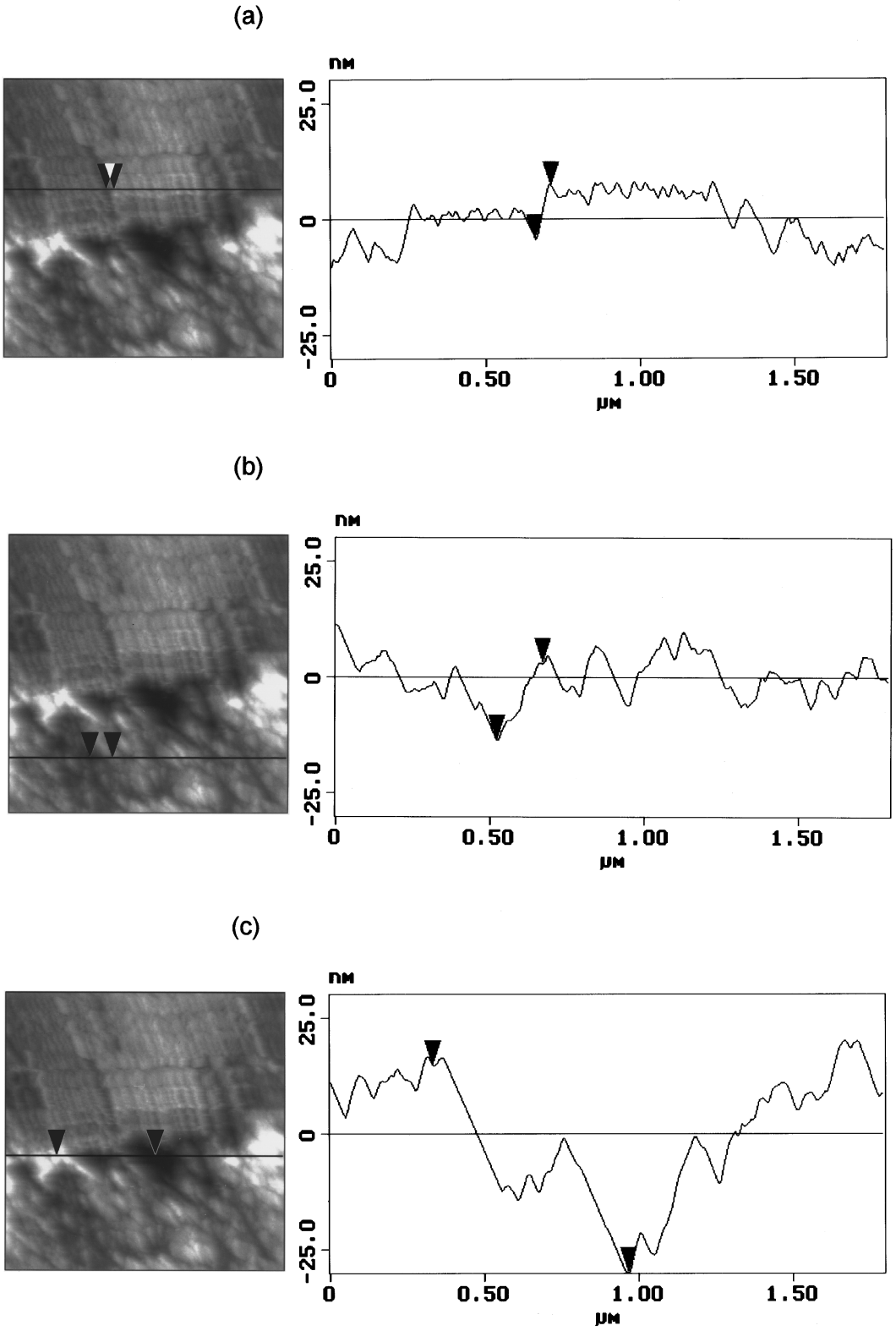

FIG. 4. Typical STM cross sections at domains I (a), II (b), and III (c).

surface atoms on Cu even at null net current, and the remarkable heterogeneous nature of Cu electrodissolution at $j = 6\ \mu\text{A cm}^{-2}$.

As far as the first issue is concerned, it should be noted that the high mobility of Cu surface atoms on Cu is comparable to that already reported for Ag surface atoms on Ag and Au atoms on Au in acid solutions.[2,30]

On the other hand, from the standpoint of roughness development at $j = 6\ \mu\text{A cm}^{-2}$, Cu exhibits a rather complex behavior where nm-sized domains at the single-crystal surface obey different dissolution modes. Thus, while for domains I and II the interface becomes rougher, domain III is characterized by a dissolution mechanism which favors deep pit growth leading to an unstable interface.

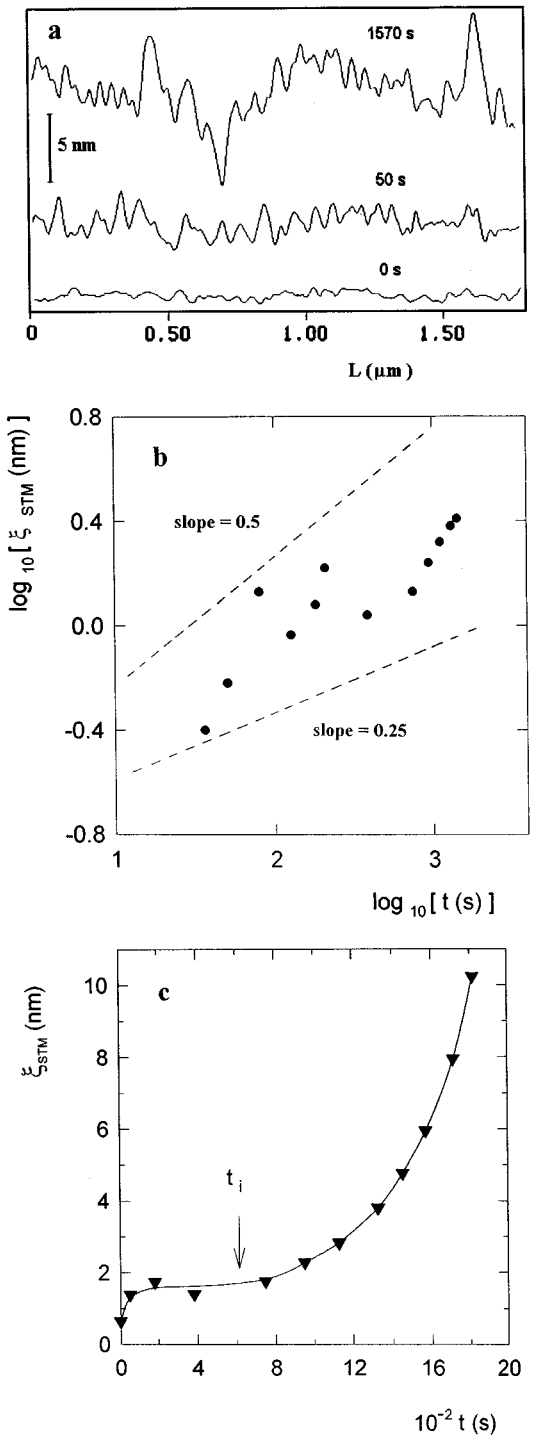

FIG. 5. (a) A typical cross-section evolution resulting from domain I. (b) A $\log_{10}\xi_{\mathrm{STM}}$ vs $\log_{10}t$ plot of domains I and II resulting from 600×600 nm^2 STM images. (c) A ξ_{STM} vs t plot resulting from the overall STM images (1700×1700 nm^2) shown in Fig. 3.

To interpret the above-mentioned results, a simple model including the stochastic nature of the dissolution process, the key role played by Cu atom surface diffusion, and the development of unstable singularities is considered. Accordingly, 3D Monte Carlo simulations from the model can be directly compared with the evolution of the Cu/aqueous $HCl0_4$ solution interface imaged by STM.

B. Monte Carlo modeling

Three-dimensional Monte Carlo simulations for the dissolution of a solid substrate were performed on the basis of the procedure already described for the two-dimensional[31] and three-dimensional cases.[19] Simulations were based on a substrate initially consisting of a cubic lattice either $60\times60\times60$, $80\times80\times26$, $90\times90\times20$, or $100\times100\times17$ in grid size. From the standpoint of particle dynamics, two principal models were considered.

In the first model (model I), the random particle detachment from the smooth substrate surface implies a site-dependent detachment probability, $P_d(N)$, given by

$$P_d(N)=6-N/5, \tag{5}$$

where N is the coordination number of the detaching particle at the substrate surface.

A more realistic dependence of the Arrhenius type

$$P_d(N)=K\ \exp(-BNE), \tag{6}$$

was also used to describe the dissolution process at different surface sites, where $B=1/k_BT$, k_B being the Boltzmann constant, and T the temperature in K. In the calculations, Eq. (6) was normalized for $N=1$. Accordingly, $P_d(1)=K/e$. As similar results were obtained using Eqs. (5) and (6), the latter involving a longer computing time, we decided to use Eq. (5) for our 3D simulations.

According to the model, after particle detachment neighbor particles around the created vacancy are allowed to diffuse on the substrate surface within a certain maximum length l_{dM} to reach a site with a higher N. The value of l_{dM} is given by

$$l_{dM}=na, \tag{7}$$

where n is an integer and a is the lattice distance. For a constant Monte Carlo time, a change in the value of l_{dM} implies a change in the surface diffusion coefficient which incorporates the activation energy for surface atom diffusion.

In the model, a restriction to the interlayer mass transport is introduced considering a probability P_{sc} that particles in the range of l_{dM} may jump down through a step edge. Thus, when $P_{sc}=0$, interlayer mass transport is completely inhibited. In this case, particles within the distance l_{dM} can move on the same terrace only in order to increase N. Otherwise, when $P_{sc}=1$, as the interlayer mass transport is permitted, particles can move freely from one terrace to another. This model accounts for the possible presence of energy barriers to surface atom diffusion at step edges.[3,32]

Monte Carlo simulations resulting from the above-mentioned model for $P_{sc}=0$, after the removal of 5.5×10^4 particles, lead to a surface consisting of smooth surface cavities. In this case, the ξ versus t plot shows a tendency to attain a certain degree of saturation when the topography approaches a single smooth surface cavity. The $\log_{10}\xi$ versus $\log_{10}t$ plot leads to $\beta=0.45$, and no change in the value of β can be observed by increasing l_{dM}. But when P_{sc} moves from 0 to 0.3, β decreases from 0.45 to 0.25. Finally, for $P_{sc}>0.3$, $\beta=0.25$ for $t\Rightarrow0$ and $\beta>0.5$ for $t\Rightarrow\infty$. Accordingly, model I with $P_{sc}<0.3$ becomes useful to describe the evolution of domains I and II [Fig. 6] as the experimental β

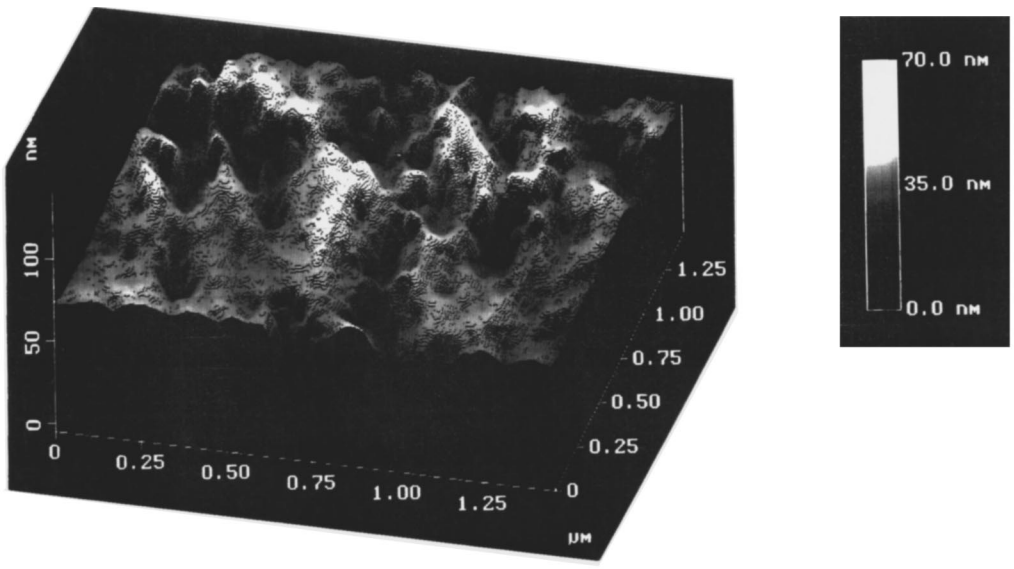

FIG. 6. An AFM $1450\times1450\ \mathrm{nm}^2$ *ex situ* image of Cu after electrodissolution in $1M$ $HClO_4$ at $j=6\ \mu\mathrm{A\ cm}^{-2}$ for 30 min.

value is comprised between 0.45 and 0.25. On the other hand, for $P_{sc}>0.3$ and $t\Rightarrow\infty$, $\beta>0.5$, as expected for interface evolution models in which a complete surface diffusion term has been incorporated into the interface motion equation.[33] In principle, it can be argued that this would be the case of domain III as $\beta>\frac{1}{2}$ for $t\Rightarrow\infty$. In this model, however, the unstable interface results from the development of shallow cavities rather than deep pits. Therefore, although model I for $P_{sc}>0.3$ and $t\Rightarrow\infty$ describes an unstable interface growth, it fails to account for the behavior of domain III.

Based on model I, a new model (model II) can be considered to simulate the electrodissolution enhancement at tip cavities caused by the presence of solid defects, such as dislocations, salt formation, localized impurities, or inhomogeneous adsorption taking place along the metal electrodissolution. In this case, for $h<h_0$, the following equation for P_d was used,

$$P_d=P_d(N)P_d(h_0-h/h_0), \tag{8}$$

consisting of two probability terms, one which depends on N, and the other which depends on h and h_0, the height of the dissolving site and the height of the highest dissolution site, respectively, measured with respect to the initial basal plane of the substrate. Equation (8) introduces the influence of a diffusion field on the detachment probability at the dissolving cavity through the term $P_d(h_0-h/h_0)$. This model originates a topography with a number of large cavities [Fig. 7(a)] which can be compared to those resulting from nanoscopy imaging (Fig. 6). Furthermore, model II predicts an increase in ξ with t [Fig. 7(b)] similar to that found from imaging data as Cu electrodissolution proceeds. Therefore, model II seems to capture the essential physics of domain III for Cu electrodissolution in the acid solution.

C. The reaction mechanism of Cu electrodissolution and the resulting surface topography

The analysis of STM imaging data from the different topographic domains resulting from Cu immersed in the aqueous environment, under $j=6\ \mu\mathrm{A\ cm}^{-2}$, show that regions of low and high dissolution rate can be distinguished, the electrodissolution reaction mainly occurring at defective sites of the Cu surface (Fig. 8). Then, the explanation of these changes in terms of a possible reaction mechanism taking place at the interface can be attempted. For this purpose, let us first consider a likely general electrodissolution reaction pathway for Cu in acid.

On the assumption that the influence of the adsorption of solution constituents at the Cu surface becomes negligible, the electrodissolution of Cu in acid can be represented by the following set of reactions:[29]

$$\mathrm{Cu}(s)=\mathrm{Cu}^{+}(\mathrm{int})+e^{-}, \tag{9a}$$

$$\mathrm{Cu}^{+}(\mathrm{int})=\mathrm{Cu}^{+}(\mathrm{bulk}), \tag{9b}$$

$$\mathrm{Cu}^{+}(\mathrm{int})=\mathrm{Cu}^{2+}(\mathrm{int})+e^{-}, \tag{9c}$$

$$2\ \mathrm{Cu}^{+}(\mathrm{bulk})=\mathrm{Cu}^{2+}(\mathrm{bulk})+\mathrm{Cu}, \tag{9d}$$

$$\mathrm{Cu}^{2+}(\mathrm{int})=\mathrm{Cu}^{2+}(\mathrm{bulk}), \tag{9e}$$

where (s) and (int) denote Cu species at the surface lattice with crystallographic indices hkl, characterized by a maximum coordination number $N=9$, and Cu species at the Cu electrolyte solution interface (electrical double-layer region), respectively. According to electrochemical kinetic data[28] Eqs. 9(a)–9(e) provide a general description for the transfer of Cu species from the solid to the bulk of the solution.

The overall electrodissolution process, in addition to Eqs. 9(a) to 9(f), also involves the participation of Cu surface atom diffusion by shifting the equilibrium between Cu surface atoms and Cu adatoms, i.e.,

$$\mathrm{Cu}(s)=\mathrm{Cu}(\mathrm{ad}) \tag{10}$$

where (ad) denotes an adsorbed Cu atom $(N\rightarrow1)$. Equation 9(a)–9(b) and Eq. (10) constitute a consortial mechanism for the Cu electrodissolution reaction which is applicable to any domain of the Cu surface. It should be noted that Eq. (10) in

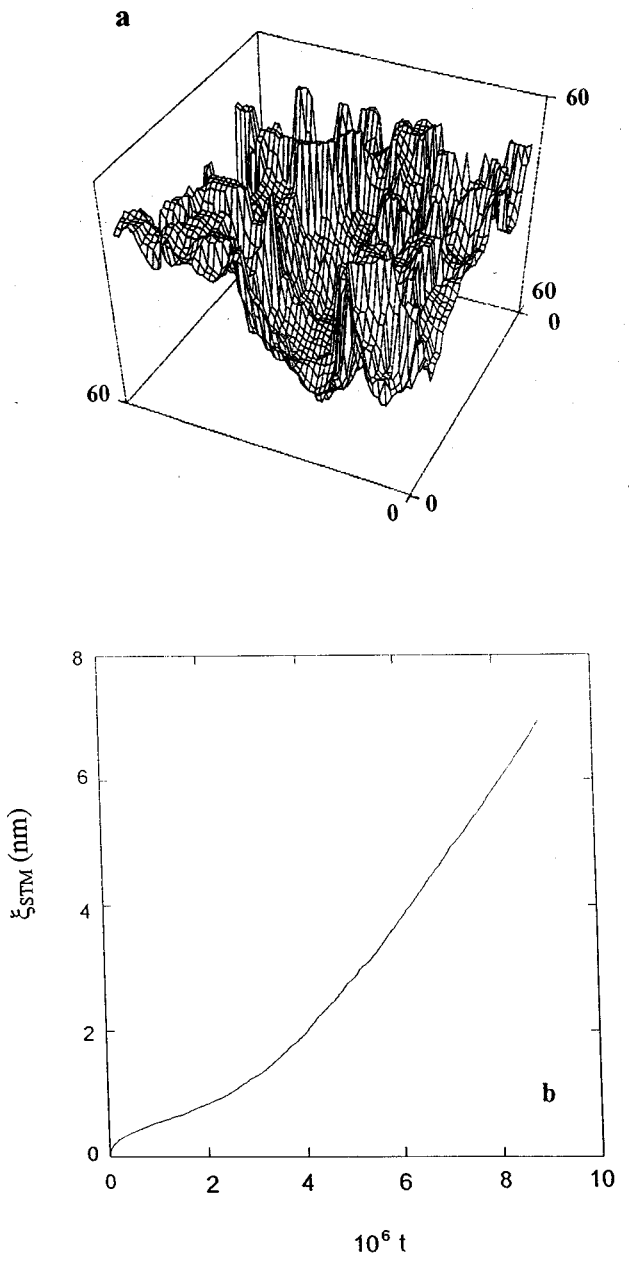

FIG. 7. A snapshot of a 3D surface resulting from the Monte Carlo simulation of model II b including adatom surface diffusion $l_{dM}=2$, $P_{sc}=0$ and stabilization at tip cavities. (b) ξ vs t plot from model II b.

the forward direction prevails when a positive potential is applied to Cu. A scheme of this complex set of equations producing a nonuniform electrodissolution of Cu is indicated in Fig. 8 where localized low and high rate electrodissolution domains are depicted, as observed in STM imaging.

To relate the development of the unstable Cu topography to the consortial mechanism discussed above, it is convenient to consider each equation step independently. Thus, Eq. (10) indicates the possibility that surface Cu atoms more strongly bound to the surface ($N \leqslant 9$) could be displaced by surface diffusion to other surface sites where $N \rightarrow 1$. Then, loosely bound Cu adatoms can be either electro-oxidized to Cu^+ ions [Eq. 9(a), first electron transfer] or displaced towards sites of higher coordination by surface diffusion [Eq. (10), backwards]. The specific rate of this equation is related, at 298 K, to $D \cong 10^{-15}$ cm^2 s^{-1}.

The origin of the driving force for the surface diffusion process could be related to either the chemical-potential gradient involving the surface energy of the different crystallographic faces, which is influenced by the solution constituents, as discussed further on, or to the surface curvature as described elsewhere.[3] Further on, Cu^+ ions can move by diffusion and migration from the reaction interface outwards [Eq. 9(b)] or they can be further electro-oxidized to Cu^{2+} ions at the interface [Eq. 9(c), second electron transfer]. In addition, the equilibrium between Cu^+, Cu^{2+}, and Cu at the equation interface is established [Eq. 9(d)].[29] Finally, Cu^{2+} species are also shifted from the interface outwards by migration and diffusion [Eq. 9(d)]. The simultaneous occurrence of this sequence of reactions at different defective surface sites produces a current flow yielding soluble Cu ionic species and localized voids at the surface. These voids contribute to the increase in the value of ξ [Fig. 5(c)].

Experimental data allow us to discriminate which of the dominant steps of the consortial reaction mechanism is responsible for the unstable surface growth range in Cu electrodissolution. Firstly, Eqs. 9(b) and 9(e), implying uniform mass transport processes should be discarded as the origin of the unstable interface, because a mass transport limited reaction Cu electrodissolution at tips should be more efficient than that at valley sites, and therefore, a leveling rather than a roughening effect would be expected. Furthermore, Eq. 9(d) occurs at rather high Cu^+ ion concentration levels leading to the formation of Cu sludge which is not observed.[28,29] Accordingly, from the standpoint of electrochemical kinetics, it appears that electrochemical equations 9(a) and 9(c), under activation control,[29] are mainly responsible for the unstable interface evolution observed in our work. This conclusion is consistent with the slope of the $\log_{10} j$ versus E plot, $b_a = 0.040$ V/decade, which was assigned to Eq. 9(c) as rate limiting.[29] The value $b_a = 0.040$ V/decade for $E > 0.17$ V allows us to conclude that unlike Ag electrodissolution,[34] when $j > 0$, the contribution of Eq. (10) to the overall kinetics of Cu electrodissolution is far from dominant. However, when the electrodissolution current is switched off ($j = 0$), the local accumulation of Cu adatoms would favor Eq. (10) in the backward direction assisting surface smoothening, as described in Sec. III B.

The preceding analysis indicates that for domains III, which are responsible for the unstable roughness regime, the Cu electrodissolution mechanism can be simplified as follows:

$$\mathrm{Cu}(hkl) = \mathrm{Cu}^+(\mathrm{int}) + e^-, \qquad (9a')$$

$$\mathrm{Cu}^+(\mathrm{int}) = \mathrm{Cu}^{2+}(\mathrm{int}) + e^-. \qquad (9c)$$

Accordingly, the overall reaction, represented by the sum of Eqs. 9(a) and 9(c), should depend on the crystallographic face of Cu, and the rate of Eq. 9(c) should depend on the concentration of Cu^+ ions at the interface.

For the development of an unstable surface at domain III let us consider the relevant steps leading to the enlargement of a local irregularity (Fig. 8, high dissolution rate domain). On extending this process to the entire surface of the elec-

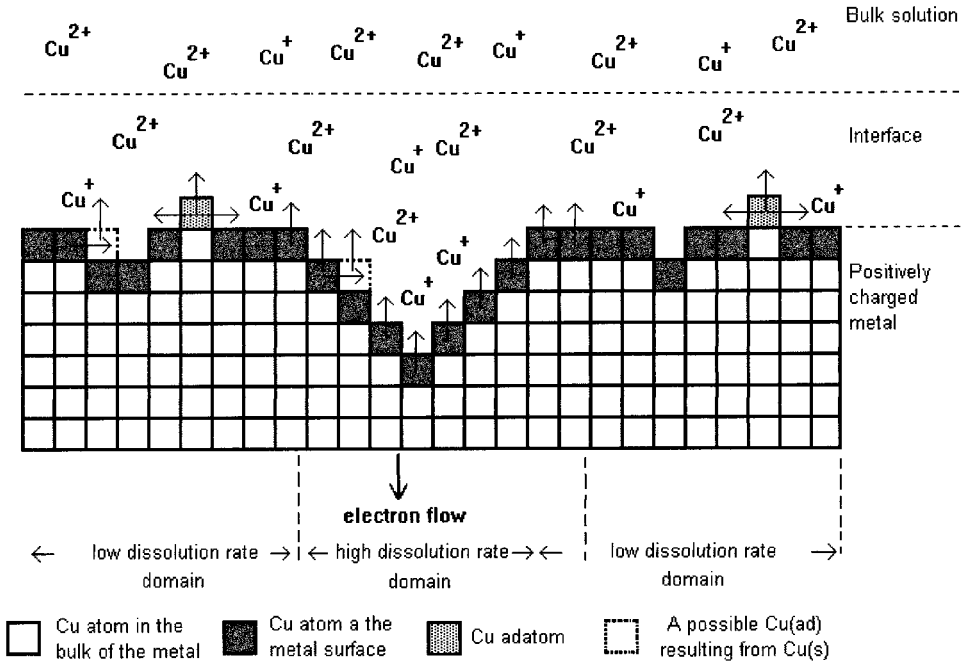

FIG. 8. A scheme of the system Cu/aqueous acid environment resulting from Eqs. 9(a)–9(e) and (10). Cu surface (2D lattice) in contact with the solution exhibiting defects where Cu electrodissolution is favored. Cu^{+} and Cu^{2+} represent soluble Cu species at the interface and bulk solution. Defective sites at the surface and domains of low and high-electrodissolution rates are shown. An arbitrary thickness of the interfacial region (int) where the electroneutrality condition is no longer obeyed is indicated by the dotted lines (anions are not indicated in the scheme). The Cu surface is positively charged for $E > E_{pzc}$. (Ref. 35) Vertical arrows upwards indicate electron transfer steps yielding Cu^{+} [Eqs. 9(a)] and Cu^{2+} [Eq. 9(c)] either directly or through Cu adatoms involved in Eq. (10) (horizontal arrows). The result of these reactions is an increase in roughness.

trodissolving metal, a number of irregularities are produced which in turn increase the number of defective sites at the surface. Then, the result is a continuous increase in surface roughness, as seen through the value of ξ, the average roughness of the sampled surface area, which increases with the electrodissolution time [Fig. 5(c)].

An unstable interface evolution at domain III could be sustained by a nonuniform Cu^{+} ion concentration profile at the interface. The origin of this nonlocal effect can be related to the large anisotropy for the Cu(111), Cu(100), and Cu(110) surfaces for both electrodissolution and electrodeposition due to the difference in their potentials of zero charge (E_{pzc}).[35] Thus, after the initial attack of the Cu surface, the different electrodissolution rates of each crystallographic plane would be reflected in stabilizing growing cavities in which the nonlocal effect manifests itself. A simple analysis of the average and local electrodissolution rates supports this possibility.[36] Thus, the value $j = 6\ \mu A\ cm^{-2}$ is equivalent to an average penetration rate of 0.012 atom/s, a figure which is almost 15 times smaller than that of 0.2 atom/s measured at cavities.

Certainly, it can be argued why Cu and Ag behave differently considering that Ag crystallographic faces exhibit differences in (E_{pzc}) (Ref. 35) similar to those in Cu. In fact, as opposed to Cu, etched pit formation in Ag electrodissolution at similar values of j has not been observed and, therefore, model I appears to be applicable.[2] However, the different behavior of Cu and Ag can be understood considering that, in constrast to Cu, the electrodissolution rate of Ag is limited by the surface diffusion of Ag adatoms, and accordingly, nonlocal effects caused by nonhomogeneous Ag^{+} ion concentration profiles are, in principle, absent.

Concerning the influence of adsorption processes involving species that are constituents of the solution, it has also been reported that competitive anion adsorption reduces step motion and promotes dissolution at surface defects leading to etched pits on Cu.[29] Furthermore, the electroformation of $Cu(OH)_{ad}$ chains on Cu has been observed by STM imaging even in acid solutions.[37,38] Then, if $Cu(OH)_{ad}$-covered terraces coexist with either uncovered or partially covered domains with weakly adsorbed ClO_4^{-} ions such as defective sites, preferential electrodissolution could also be favored. Thus, either a nonhomogeneous adsorption or electroadsorption of species from the solution side at distinct crystallographic defects could be another possible origin of unstable surface growth for Cu in the acid solution. This possibility is supported by the fact that in acid solutions containing 10^{-4}–10^{-3}M HCl, Cu electrodissolution at low j largely proceeds from step edges[39] without a remarkable change in the value of ξ_{STM}.[40] In this case, a monolayer of adsorbed Cl^{-} ions[39] could reduce nonhomogeneous adsorption and accordingly, unstable interface evolution will no longer be observed.

ACKNOWLEDGMENTS

This work was financially supported by the Consejo Nacional de Investigaciones Científicas y Técnicas of Argentina (CONICET) and the Third World Academy of Sciences (TWAS) Associate Membership Scheme at Centres of Excellence in the South.

*Permanent address: Department of Chemistry, University of King Abdulaziz, Jeddah, Saudia Arabia.
†Permanent address: Departamento de Quilmica-Fisica, Universidad de La Laguna, Tenerife, Spain.

[1] G. Daccord, in *The Fractal Approach to the Heterogeneous Chemistry*, edited by D. Avnir (Wiley, New York, 1989), p. 183.
[2] M. E. Vela, G. Andreasen, R. C. Salvarezza, A. Hernández Creus, and A. J. Arvia, Phys. Rev. B **53**, 10 217 (1996).
[3] A. L. Barabási and H. E. Stanley, *Fractal Concepts in Surface Growth* (Cambridge University Press, New York, 1995).
[4] W. H. Smyrl, in *Comprehensive Treatise of Electrochemistry*, edited by J. O'M. Bockris, B. E. Conway, E. Yeager, and R. E. White (Plenum, New York, 1981), Vol. 4, p. 97.
[5] N. Sato and G. Okamoto, in *Comprehensive Treatise of Electrochemistry* (Ref. 4), Vol. 4, p. 193.
[6] M. G. Fernandes, R. M. Latanision, and P. C. Searson, Phys. Rev. B **47**, 11 749 (1993).
[7] J. G. Armar and F. Family, Phys. Rev. Lett. **64**, 543 (1990).
[8] B. Grossman, H. Guo, and G. Martin, Phys. Rev. A **43**, 1727 (1991).
[9] T. Hwa, M. Kardar, and M. Paczuski, Phys. Rev. Lett. **66**, 441 (1991).
[10] J. D. Weeks and G. H. Gilmer, Adv. Chem. Phys. **40**, 157 (1979).
[11] C. S. Kohli and A. W. Ives, J. Cryst. Growth **16**, 123 (1972).
[12] K. W. Cheng and A. W. Coller, J. Cryst. Growth **84**, 436 (1987).
[13] K. Sieradzki, R. R. Corderman, K. Shukla, and R. C. Newman, Philos. Mag. A **4**, 713 (1989).
[14] F. Family, Physica A **168**, 561 (1990), and references therein.
[15] J. Krug and H. Spohn, in *Solids Far From Equilibrium. Growth, Morphology and Defects*, edited by C. Godreche (Cambridge University Press, Cambridge, England, 1990).
[16] *Dynamics of Fractals Surfaces*, edited by F. Family and T. Vicsek (World Scientific, Singapore, 1991).
[17] R. C. Salvarezza, L. Vázquez, P. Herrasti, P. Ocón, J. M. Vara, and A. J. Arvia, Europhys. Lett. **20**, 727 (1992).
[18] L. Vázquez, R. C. Salvarezza, P. Herrasti, P. Ocón, J. M. Vara, and A. J. Arvia, Appl. Surf. Sci. **70**, 413 (1993).
[19] A. Hernández Creus, P. Carro, R. C. Salvarezza, and A. J. Arvia, Langmuir **13**, 833 (1997).
[20] X. G. Zhang and U. Stimming, J. Electroanal. Chem. **291**, 273 (1990).
[21] D. M. Kolb, R. J. Nichols, and R. J. Behm, in *Electrified Interfaces in Physics, Chemistry and Biology, NATO Advanced Study Institute, Series C:* edited by R. Guidelli (Kluwer Academic, Dordrecht, 1992), p. 275.
[22] J. E. T. Andersen, G. Bech-Nielsen, P. Moeller, and J. C. Reeves, J. Appl. Electrochem. **26**, 161 (1996).
[23] R. M. Rynders and R. C. Alkire, J. Electrochem. Soc. **141**, 1166 (1994).
[24] R. J. Nichols, W. Beckmann, H. Meyer, N. Batina, and D. M. Kolb, J. Electroanal. Chem. **330**, 381 (1992).
[25] J. Y. Josefowicz, L. Xie, and G. C. Farrington, J. Phys. Chem. **97**, 11 995 (1993).
[26] A. Iwamoto, T. Yoshinobu, and H. Iwasaki, Phys. Rev. Lett. **72**, 4025 (1994).
[27] B. J. Cruickshank, A. A. Gewirth, R. M. Rynders, and R. C. Alkire, J. Electrochem. Soc. **139**, 2829 (1992).
[28] J. Krim, I. Heyvaert, C. Van Haesendonck, and Y. Bruynseraede, Phys. Rev. Lett. **70**, 57 (1993).
[29] U. Bertocci and D. R. Turner, in *Encyclopedia of the Electrochemistry of the Elements*, edited by A. J. Bard (Dekker, New York, 1974), Vol. 2, p. 383.
[30] N. Ikemiya, M. Nishide, and S. Hara, Surf. Sci. **340**, L965 (1995).
[31] A. Hernández Creus, P. Carro, R. C. Salvarezza, and A. J. Arvia, J. Electrochem. Soc. **142**, 3806 (1995).
[32] Z. Zhang, J. Detch, and H. Matiu, Phys. Rev. B **48**, 4972 (1993).
[33] F. Family, in *Fractals in the Natural and Applied Sciences*, edited by M. M. Novak (North-Holland, Amsterdam, 1994), p. 1.
[34] A. V. Vvedenskii and I. K. Marshakov, Russ. J. Electrochem. **31**, 234 (1995).
[35] M. A. Vorotyntsev, in *Moderns Aspects of Electrochemistry*, edited by J. O'M. Bockris, B. E. Conway, and R. E. White (Plenum, New York, 1986), Vol. 17, p. 131; A. Hamelin, in *Modern Aspects of Electrochemistry*, edited by B. E. Conway, R. E. White, and J. O'M. Bockris (Plenum, New York, 1985), Vol. 16, p. 1.
[36] D. Barkey, F. Oberholtzer, and Q. Wu, Phys. Rev. Lett. **75**, 2980 (1995).
[37] J. R. LaGraff and A. A. Gewirth, Surf. Sci. **326**, L461 (1995).
[38] J. R. LaGraff and A. A. Gewirth, in *Nanoscale Probes of the Solid/Liquid Interface*, Vol. 288 of *NATO Advanced Study Institute Series E*, edited by A. A. Gewirth and H. Siegenthaler (Kluwer Academic, Dordrecht, 1995), p. 83.
[39] D. W. Suggs and A. J. Bard, J. Am. Chem. Soc. **116**, 10 725 (1994).
[40] M. E. Vela, S. G. Aziz, G. Andreasen, R. C. Salvarezza, and A. J. Arvia, Electrochim. Acta (to be published).